J. Fluid Mech. (1976), *vol.* 74, *part* 4, *pp.* 611–640
Printed in Great Britain

A macromolecule transport model for the arterial wall and endothelium based on the ultrastructural specialization observed in electron microscopic studies

By SHELDON WEINBAUM

Department of Mechanical Engineering, The City College of The City University of New York, New York 10031

AND COLIN G. CARO

Physiological Flow Studies Unit, Department of Aeronautics, Imperial College, London

(Received 31 March 1975 and in revised form 15 September 1975)

A composite hydrodynamic–diffusion model of the arterial wall is presented to describe the vesicular transport of relatively inert macromolecules across the inner endothelial lining of the larger arteries of humans and animals and their subsequent diffusion in the underlying tissue of the intima and media. This model is motivated by the highly specialized ultrastructure of the arterial wall observed in electron microscopic studies and the recent experimental measurements of the time-dependent uptake of labelled macromolecules in animal arteries under carefully controlled *in vitro* conditions. The proposed dynamic model for the vesicular transport across the endothelial cell layer considers the constrained Brownian diffusion of 700 Å vesicles subject to long-range hydrodynamic and short-range London–van der Waals force interactions with the plasmalemma membranes of the endothelial cell. Approximate solutions are developed for the motion and the steady-state vesicle density distribution near the plasmalemma and in the interior of the cell using boundary-layer-like methods. The model for the vesicular transport just described appears as a novel boundary condition in the basic diffusion model for the underlying tissue. The latter is treated as a two-phase medium comprised of an interstitial fluid continuum with a uniformly dispersed smooth muscle phase as first proposed by Hills (1968). This model for the underlying tissue assumes that the smooth muscle cells contribute insignificantly to the macromolecule diffusion across the arterial wall but act as the principal storage reservoir for the macromolecules for large diffusion times because of their large volume fraction. The dimensionless parameters that arise in the theoretical model are determined by comparing the solutions for the time-dependent total wall uptake with Fry's (1973) experimental data for canine carotid artery.

1. Introduction

The passage of macromolecules across the arterial endothelium and their transient uptake by the underlying arterial wall substance have been the subject of numerous *in vivo* and *in vitro* experiments, e.g. by Adams, Morgan & Bayliss (1970), Bell, Adamson & Schwartz (1974), Bell, Gallus & Schwartz (1974), Somer & Schwartz (1971), Fry (1968, 1972, 1973), Caro, Fitz-Gerald & Schroter (1971), Caro (1973, 1974), Caro & Nerem (1973) and Caro, Siflinger & Parker (1975), numerous electron microscopic studies, e.g. by Karnovsky (1967), Casley-Smith (1964, 1969), Casley-Smith & Chin (1971), Jennings & Florey (1967), Bruns & Palade (1968), Simionescu, Simionescu & Palade (1973) and Stein & Stein (1973), and numerous theoretical models, e.g. by Shea, Karnovsky & Bossert (1969) and Shea & Bossert (1973), to mention a few representative recent investigations. These studies have been motivated in large measure by the possibly great importance that the transport of low density lipoproteins between the arterial lumen and the arterial wall might play in the incipient formation of atheromatous lesions in the larger arteries of humans and animals. This transport of macromolecules is also of general interest in the metabolism of the arterial wall. The large body of experimental and observational evidence already gathered strongly suggests that the fundamental transport mechanisms present, which appear to be closely related to the highly specialized ultrastructure of the arterial endothelium and intima, provide a fertile area for new conceptual and quantitative theoretical models on the part of the fluid dynamicist. These experiments show that the rate of macromolecule transport is sensitive to a variety of mechanical factors such as flow, pressure oscillations, sinusoidal stretch and temperature changes, although the basic mechanisms for this enhancement remain to be elucidated. In the present paper a new hydrodynamic diffusion model is developed which describes the macromolecule transport across the arterial wall and its endothelium under the static loading conditions frequently encountered in *in vitro* perfusion experiments.

Figure 1(*a*) (plate 1) is a relatively low magnification (17 000 ×) transmission electron micrograph showing a small portion of the cross-section of a canine carotid artery which has been fixed at a transmural pressure of 100 mm Hg. Proceeding inwards from the lumen one observes an endothelial cell with its nucleus, an underlying band of connective tissue, the internal elastic lamella, visible as a white layer, and finally, in the lower right-hand corner, the beginning of the arterial media, showing the interstitial fluid space and the roughly cuboidal smooth muscle cells. The arterial intima and media, which together comprise the bulk of the wall substance, contain many such layers of muscle cells. Their combined thickness for the specimen shown is roughly 2000 times the average thickness 3200 Å of the single layer of endothelial cells at the luminal surface. Figure 1(*b*) (plate 1) is a higher magnification (65 000 ×) transmission electron micrograph of the border region of two overlapping endothelial cells. The two important ultrastructural features visible in this figure are the tortuous extracellular channel separating the two cells, whose width varies between approximately 100 and 200 Å, and the numerous nearly spherical vesicles of typical

diameter 700 Å. When free, these vesicles undergo a diffusional migration across the cell which is strongly influenced by a hydrodynamic and molecular force interaction with the plasmalemma membranes of the endothelial cell and perhaps to a lesser extent by interaction with other vesicles. When attached to the plasmalemma of the endothelial cell, the vesicles are open to the luminal fluid and form a continuous part of the 75 Å molecular phospholipid bilayer structure of the plasmalemma membrane.

As first hypothesized by Palade (1960) and since confirmed by time-dependent electron microscopic tracer studies by Casley-Smith & Chin (1971) and Simionescu *et al.* (1973), the macromolecules are transported across the cell by the vesicles, which perform a ferryboat function. This process, called vesicular transport, proceeds in both directions. The vesicles fill in their open attached state, break off from their attaching stalks, migrate across the endothelial cell and reattach at the opposite plasmalemma, where they unload their contents. The time-dependent ultrastructural studies just mentioned reveal that the vesicles are attached long enough at both the luminal and abluminal surfaces to come to concentration equilibrium with the surrounding luminal and interstitial fluid respectively and that the macromolecules do not escape from the membrane-bound vesicles during their journey across the cell.

The vesicles are seldom seen in the process of rupturing or attaching so it must be assumed that the characteristic time for this process is small compared with the average attachment time t_a and the diffusion time t_D required to cross the cell. The numerous depressions visible in the scanning electron micrograph of the endothelial surface (figure 1*c*, plate 1) strongly suggest that short-range molecular forces of attraction play an important role as the vesicle approaches the plasmalemma prior to reattachment. Electron microscopic studies (Jennings & Florey 1967) and perfusion experiments (Caro *et al.* 1975) with various metabolic poisons indicate that both the driving forces for the migration of the free vesicles and the rupture of the attached vesicles are passive in that their energy derives from mechanical as opposed to metabolic factors. The diffusional migration in the intracellular fluid would appear to be a Brownian motion arising from random thermal collisions. The characteristic time, velocity and distance typifying the random vesicle motions is derived in the next section. These calculations suggest that the rupture of the vesicle stalk in the attached state might be due to a small amplitude instability in the equilibrium force balance of the attached vesicle.

Returning to the description of the intima, one observes in figure 1 (*a*) that the interstitial fluid gap between adjacent smooth muscle cells is typically of the order of several thousand Å and thus more than an order of magnitude larger than either the dimensions of the low density lipoprotein molecules or the width of the intercellular channels between adjacent cells in the endothelial cell layer. Electron microscopic tracer studies (Karnovsky 1967) show that the largest molecules which can pass through the tightest constrictions in the intercellular cleft are approximately 40 Å in radius. Thus, from the standpoint of the diffusion of macromolecules whose effective hydrodynamic radius is between 40 and 200 Å (the upper limit is determined by the internal diameter of the vesicle attachment stalks) the ultrastructure of the endothelium and the arterial intima are polar

opposites. In the arterial endothelium these macromolecules encounter a nearly infinite resistance in passing through the narrow intercellular space between the endothelial cells and traverse this layer primarily via the passive transport of the 700 Å vesicles described previously. In contrast, in the intima the macromolecules, once released by the attaching vesicles at the abluminal membrane, encounter a much smaller diffusional resistance in passing via the interstitial fluid between adjacent muscle cells than traversing the muscle cells themselves through vesicular transport or membrane diffusion. The macromolecules thus essentially bypass the dispersed cellular phase on the time scale of the characteristic interstitial fluid diffusion time. The dispersed cellular phase therefore contributes insignificantly to the diffusion across the arterial wall, but is probably the principal storage reservoir for the macromolecules for large times since its volume is roughly five times that of the interstitial fluid phase. This conceptual model of cellular tissue structure was first proposed by Hills (1968, 1970) in his studies of the uptake of gas molecules in lung capillaries and the passage of small solutes into the arterial wall. In the latter application all the complications introduced by the vesicular transport across the arterial endothelium, the essential feature of the macromolecule transport problem, can be neglected since these small molecules can easily pass through the intercellular clefts, whose permeability for small molecule transport is at least two orders of magnitude larger than that of the vesicular transport route.

In the context of the overall mathematical model for the artery wall, the vesicular transport model for the endothelial cell layer appears as a novel boundary condition in the larger-scale model for the underlying tissue. While the ultrastructural studies of the endothelial cell layer have added immeasurably to our understanding of the vesicular transport process, these studies do not currently provide reliable quantitative measurements of the vesicle dynamics because of the difficulty in accurately determining how long it takes the fixative when injected in the circulation to reach the local tissue of interest and how quickly the fixation process proceeds. For example, observational estimates by different investigators of the average transendothelial diffusion time t_D, the quantity of perhaps greatest interest in the vesicle transport studies, have differed by more than an order of magnitude, the recent studies of Casley-Smith & Chin (1971) and Simionescu *et al.* (1973) suggesting 3 and 60 s respectively. A further complication is that most of the existing literature has concentrated on capillary endothelium, whose internal structure is significantly different from that of the arterial endothelium considered herein. For these reasons a new series of time-dependent ultrastructural studies is being planned by the authors in collaboration with Drs G. E. Palade and N. and M. Simionescu. A promising new procedure for estimating t_D, which is based on the composite hydrodynamic–diffusion model of the arterial wall and endothelium and the more accurate quantitative measurements presently available from macroscopic uptake studies with labelled albumin, is described in § 5.

The next section presents a preliminary theoretical picture of the vesicle mechanics. Section 3 describes the basic dynamic model for the vesicular transport. Section 4 incorporates this vesicle transport model into the overall two-

phase diffusion model of the arterial wall. The theoretical solutions are presented in § 5 and compared with Fry's (1973) data for the time-dependent uptake of labelled albumin in normal and injured carotid artery preparations. Section 6 discusses future and related work.

2. Preliminary theoretical considerations

As a preliminary to the dynamic models of the vesicle diffusion presented in § 3, we shall first perform some simple calculations to estimate the characteristic velocity, distance and time of the individual excursions in the Brownian walk and briefly describe the existing statistical theories of the vesicle migration.

The equation of motion describing the dynamic force balance on an individual neutrally buoyant vesicle in the interior of a cell is given approximately by

$$m\frac{d\bar{u}}{dt} = -m'\frac{d\bar{u}}{dt} - 6\pi\mu a\lambda\bar{u} - 6a^2(\rho\mu\pi)^{\frac{1}{2}}\int_0^t \frac{d\bar{u}}{d\tau}\frac{d\tau}{(t-\tau)^{\frac{1}{2}}} + \bar{F}_{VW} - 6\pi\mu a\lambda D\bar{\nabla}C + \bar{G}\,\delta(t_i), \tag{2.1}$$

where $\bar{u}$, m and a are the velocity, mass and radius of the vesicle, ρ is the intracellular fluid density, which is assumed to be equal to the vesicle density, m' is the virtual mass of the vesicle ($m' = \frac{1}{2}m$ for an isolated sphere in an infinite fluid), μ is the intracellular viscosity, λ is a hydrodynamic interaction parameter, which depends on the flow geometry, D and c are the diffusion coefficient and concentration of the vesicles, $\bar{F}_{VW}$ is the van der Waals attractive force between the vesicles and the cell membrane and $\bar{G}\,\delta(t_i)$ is the impulsive force arising from random thermal collisions at times t_i, where $\delta(t_i)$ is the Dirac delta function. The forces on the right-hand side of (2.1) in the order in which they appear are the virtual mass force, the Stokes drag force, the Basset force, the integrated London–van der Waals intermolecular force, the concentration driving force and the impulse force due to molecular collisions.

On the shortest time scale, that of molecular collision, the impulse force accelerates the vesicle to its random thermal velocity. If the vesicle is in thermodynamic equilibrium with its surroundings, the average thermal speed of the vesicle u_0 after collision is given by $(3\kappa T/m)^{\frac{1}{2}}$, where κ is Boltzmann's constant and T is the absolute temperature. The thermal speed at 37 °C of a 700 Å vesicle whose density is that of water is roughly 30 cm/s.

Having been impulsively accelerated to the thermal speed u_0, the vesicle is now decelerated by Stokes frictional resistance forces. A rough engineering estimate of the duration and the distance travelled in the ensuing motion can be obtained by neglecting all but the first two terms on the right-hand side of (2.1) and letting $\lambda = 1$ and $m' = \frac{1}{2}m$, their values for an isolated sphere in an infinite fluid:

$$m\,du/dt = -\tfrac{1}{2}m\,du/dt - 6\pi\mu ua. \tag{2.2}$$

The integral of (2.2) that satisfies the initial condition $u_0 = (3\kappa T/m)^{\frac{1}{2}}$ is

$$U = \left(\frac{3\kappa T}{m}\right)^{\frac{1}{2}}\exp\left(-\frac{4\pi\mu a}{m}t\right). \tag{2.3}$$

The distance travelled from the point of collision $x = 0$ is

$$x = \frac{(3m\kappa T)^{\frac{1}{2}}}{4\pi\mu a}\left[1 - \exp\left(-\frac{4\pi\mu a}{m}t\right)\right]. \tag{2.4}$$

The exponential decay time t_e and the total distance x_e travelled before the vesicle comes to rest ($t = \infty$) are, from (2.3) and (2.4),

$$t_e = m/4\pi\mu a = \rho a^2/3\mu, \tag{2.5}$$

$$x_e = \frac{(3m\kappa T)^{\frac{1}{2}}}{4\pi\mu a} = \left(\frac{\rho a \kappa T}{4\pi\mu^2}\right)^{\frac{1}{2}}, \tag{2.6}$$

where $m = \frac{4}{3}\pi\rho a^3$. There is at present no reliable measurement of the intracellular viscosity of endothelial cells. Values used previously in the literature (Irani & Adamson 1958; Taylor 1965; Green & Casley-Smith 1972) span the range 0·1–1·0 P. The corresponding values of t_e and x_e are $3 \times 10^{-12} < t_e < 3 \times 10^{-11}$ s and $0{\cdot}09 < x_e < 0{\cdot}9$ Å.† Thus the motion is extremely short lived and has an amplitude which is small compared with the vesicle dimensions. In contrast, the Brownian motion of 1 μm particles, which are readily observed in optical microscopy, shows deflexions which are of the same order as the particle dimensions.

The above crude calculations provide some insight into the possible nature of the vesicle rupture process. The vesicle is a rather thick-walled structure, its interior fluid contents comprising only about 48 % of its total volume. An attached thick-walled structure of this type is not likely to migrate far from its equilibrium position under the influence of many small displacements. This conclusion is supported by electron micrographs, which rarely show the vesicle stalks to be highly distorted from their mean attached configuration. The most likely explanation of the vesicle release is that it is a fracture due to small amplitude impulsive loading. A reasonable hypothesis is that the vesicle's dimensions and its attached configuration are determined by membrane bending stresses in equilibrium with membrane electrical forces of London–van der Waals type, and that this equilibrium is unstable to small amplitude, high frequency disturbances such as thermal collisions. The increased uptake of labelled albumin with increasing temperature (Caro *et al.* 1975) and the preliminary small amplitude stretch studies performed by the authors in Caro, Lewis & Weinbaum (1974) are consistent with this hypothesis. In the latter study excised artery segments were subjected to pulsed and sinusoidal small amplitude elongations of the same frequency and amplitude. The pulsed specimens showed only a marginal increase above controls, whereas the sinusoidally stretched segments experienced a near doubling in uptake. Since intracellular motions decay almost instantaneously after each pulse [this time is of the same order as t_e in (2.5)], this suggests that the increased uptake in the sinusoidally stretched segments is due to a decrease in the vesicle diffusion time t_D rather than the attachment time t_a. The fact that t_a is unaffected is consistent with the above discussion since the boundary velocities

† *Note added in proof.* Equation (2.6) significantly underestimates the amplitude of a Brownian excursion because it neglects the Basset force term in (2.1). More accurate approximations to (2.1) which include the Basset force are currently being studied. These results show that the above values for x_e are one to two orders of magnitude too small.

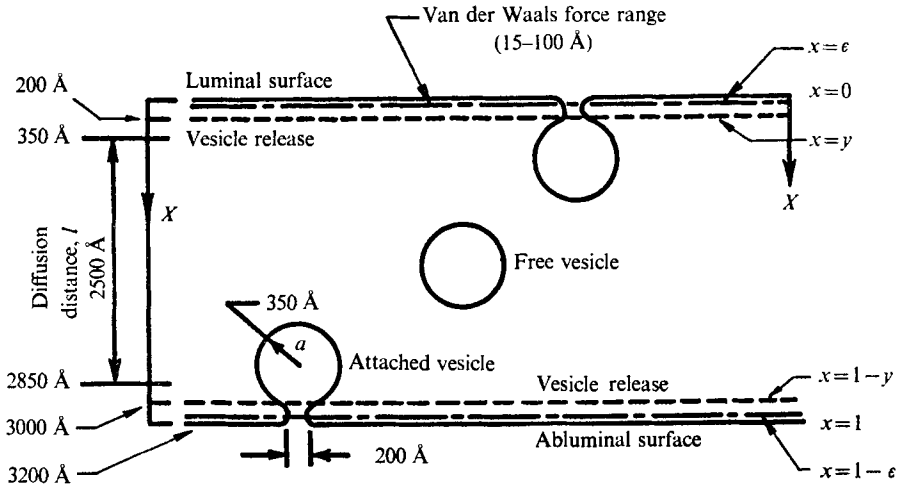

FIGURE 2. Schematic illustration showing co-ordinates and geometry for mathematica model of plasmalemma vesicle migration across border region of endothelial cell. Dimensions shown based on canine carotid artery.

generated in the pulsed case were still at most two orders of magnitude smaller than the random thermal velocity of the vesicles.

The two fundamental physical features of the present vesicle diffusion problem that greatly complicate its dynamics are (i) that the vesicle is undergoing a very strong, spatially varying, hydrodynamic interaction with the plasmalemma membranes of the endothelial cell since its diameter 700 Å is nearly a quarter of the average total intracellular diffusion distance 3200 Å across the endothelial cell, and (ii) that the vesicle is released sufficiently close to the boundary (the intrusion distance is approximately 200 Å; Shea *et al.* 1969) for lubricating film and van der Waals intermolecular force interaction effects to be important.† A schematic illustration of the border region of an endothelial cell showing the pertinent dimensions and geometry for the vesicle diffusion problem is given in figure 2.

While no dynamic model has been proposed to deal with the constrained Brownian diffusion problem just described, several statistical theories have been advanced based either on a continuum diffusion equation with uniform diffusivity (Tomlin 1969; Shea *et al.* 1969; Shea & Bossert 1973) or on a kinetic theory of

† The exterior surfaces of many biological membranes have a small negative surface charge which in the presence of an ionic suspending medium causes an electric double layer to form in the vicinity of the surface. The extra-cellular channel is very likely due to a balance between the repulsive forces caused by this negative surface charge and the attractive van der Waals forces. Much less is known about the membrane electrical properties in the interior of the cell. Very high magnification electron micrographs indicate that there is no equilibrium gap between the vesicle and the plasmalemma membrane prior to attachment, see sketch in figure 3(*c*). This suggests that either electrical double layers are not present or non-uniformly distributed on the interior surface of the plasmalemma or that the surface charges are of opposite sign. In this first model these surface electrical effects will not be considered, although this aspect of the model warrants more careful study.

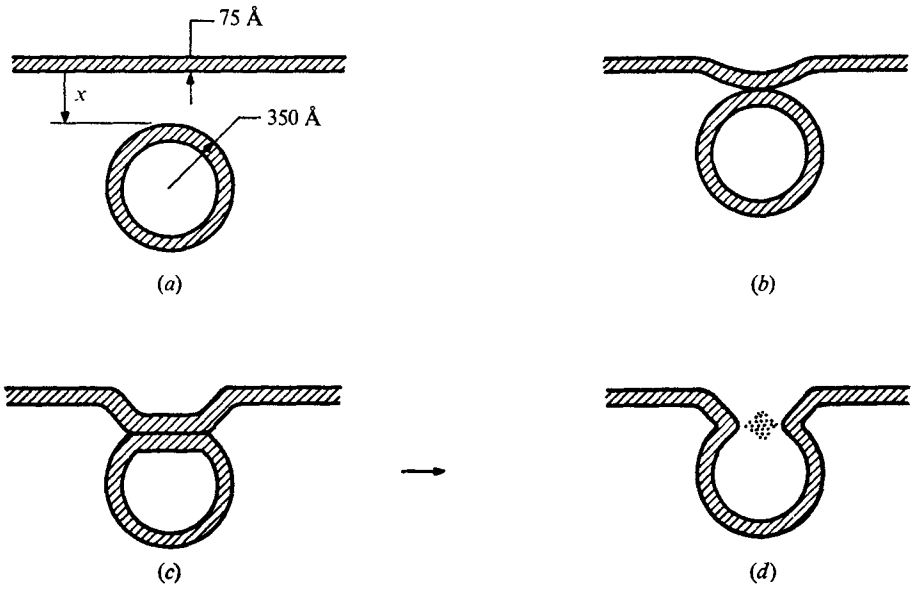

FIGURE 3. Sketch of proposed sequence of events leading to reattachment of free vesicles to plasmalemma membrane. (*a*) $x > 200$ Å, hydrodynamic interaction. (*b*) $x < 200$ Å, hydrodynamic–van der Waals interaction. (*c*) Before stalk formation. (*d*) Reattached configuration.

liquids approach (Green & Casley-Smith 1972). In Shea *et al.* the importance of a finite intrusion distance or vesicle stalk length is recognized, since if the vesicle were released right at the plasmalemma, energy would be required to prevent it from immediately reattaching to this surface. The inadequacy of the simple statistical models presented in Tomlin (1969) and Shea *et al.* (1969), which predict a linear vesicle concentration profile across the endothelial cell, is clearly demonstrated in the time-dependent electron microscopic tracer studies of Casley-Smith & Chin (1971) and Simionescu *et al.* (1973). Both these observational studies show that in the steady state the density profile of labelled vesicles crossing from the luminal to the abluminal surface changes much more gradually in the interior of the cell than near the plasmalemma on either side of the endothelial cell, suggesting that the plasmalemma exhibits repulsive properties.

Shea & Bossert (1973) and Green & Casley-Smith (1972) attempt to explain the more uniform distribution of vesicles in the cell interior by introducing a phenomenological wall reflexion coefficient. Shea & Bossert modify the theoretical model in Shea *et al.* (1969) by changing the wall boundary condition from that of a perfectly absorbing membrane to that of an imperfectly absorbing 'elastic' barrier. This new model assumes that the vesicles have a finite probability of being repelled by the wall, in which case they are instantaneously returned some small specified distance into the interior of the cell. Green & Casley-Smith present a higher-order kinetic-theory approximation to the diffusion equation which includes a first-order correction for vesicle–vesicle interactions in more dense systems. However, the basic problem, the description of the vesicle motion in the vicinity of the boundary, is treated in an even more approximate manner

than by Shea & Bossert (1973), where the important concept of a finite intrusion distance is retained in the statistical model.

The basic hypothesis that the plasmalemma is an imperfectly absorbing barrier from which the vesicle is repelled by molecular forces is not consistent with the appearance of the plasmalemma surface in figure 1(*c*) nor with current molecular models of the London–van der Waals electrical forces that are operative between biological membranes over distances between roughly 10 and 200 Å. The usually accepted view is that these forces are attractive rather than repulsive in nature except for very short range molecular interactions, over less than 5–10 Å, where very strong nuclear repulsive forces start to dominate; see for example Israelachvili & Tabor (1972).

The authors have recently had the opportunity to examine the extensive collection of very high magnification transmission electron micrographs taken by Dr G. E. Palade and co-workers. Figure 3 is a schematic illustration constructed from many electron micrographs of the sequence of events leading to the attachment of a free vesicle to the plasmalemma. When the fluid gap x between the vesicle and the plasmalemma is greater than approximately 200 Å the nearly spherical vesicle is being acted upon principally by concentration-gradient and hydrodynamic resistance forces, as shown in sketch (*a*). Since the hydrodynamic resistance force which must be overcome to squeeze out of the thin fluid layer between the vesicle and the plasmalemma is proportional to a/x for small gap widths, this force starts to grow very rapidly as the gap width decreases to less than a vesicle radius and is very likely responsible for the repulsive character of the plasmalemma suggested by the labelled vesicle density profile. In sketch (*b*) the vesicle has approached close enough to the plasmalemma for the London–van der Waals molecular attractive force between the vesicle and plasmalemma membranes to be important. While the non-retarded attractive potential between individual molecules behaves as $1/r^6$, we shall show in the next section that the integrated attractive force summed over all interaction pairs behaves as $1/x^4$ and thus must overwhelm the hydrodynamic resistance force for small enough gap widths. In the limit as x approaches zero the molecular attractive forces eliminate the fluid gap entirely, as shown in sketch (*c*). Owing to the curvature of the vesicle, a large spatially varying stress is produced on both the vesicle and the plasmalemma membrane by the local hydrodynamic and molecular forces. The vesicle, being a relatively thick-walled structure, does not deform easily, whereas the plasmalemma first indents and then applanates as shown in sketches (*b*) and (*c*). The adhered configuration (*c*) is not stable at the molecular level and rapidly changes into the attached configuration (*d*). Very detailed examination of the transition to the attached configuration suggests that there is a radial outflow of membrane material with a small lipid remnant which is thickest in the centre of the newly formed stalk. This remnant appears to be short lived compared with the average life span t_a of the vesicle in the attached state. It is reasonable to speculate that the molecular attractive forces acting across the neck of the vesicle provide a ring-like constraint which prevents the vesicle from disappearing entirely as a planar portion of the plasmalemma.

3. Dynamic models of the vesicle motion

It is evident from the remarks of the previous section and the dimensions shown in figure 2 that the vesicle motion is characterized by two different length scales: a short length ϵ_0, representative of London–van der Waals electrical forces, and a long length l, representative of hydrodynamic interaction forces, which in the present case can be taken as the transendothelial diffusion distance between the plasmalemma membranes. The mathematical model on the short length scale describes the final approach of the vesicle to the plasmalemma under the influence of concentration-gradient, hydrodynamic resistance and London–van der Waals forces. This model is used to define an effective cut-off distance for the van der Waals forces, which can be thought of as the apparent boundary for the diffusion model in the interior of the cell. The second model provides an accurate description of the spatially varying long range hydrodynamic interaction with both boundary membranes, but approximates the effect of the van der Waals force near the plasmalemma by the use of the effective cut-off distance just mentioned.

3.1. *Vesicle motion near plasmalemma*

Our first objective in this section is to develop an approximate mathematical model which describes the transition from the hydrodynamic–concentration-gradient force balance in the interior of the cell to the hydrodynamic–van der Waals force balance that holds as the vesicle approaches the plasmalemma prior to reattachment. This transition occurs over a length scale which is probably of the order of 200 Å and involves maximum velocity changes which are one to two orders of magnitude larger than the macroscopic diffusion velocity of the vesicle. Since this distance is large compared with the viscous stopping distance of a vesicle impulsively accelerated by thermal collisions [equation (2.6)], and the velocity is small compared with the random thermal velocity of the vesicle, it is reasonable to neglect the unsteady inertia and Basset force terms in the dynamic equation of motion (2.1) of the vesicle. The instantaneous quasi-steady-state force balance on the vesicle from (2.1) is given by

$$0 = F_{VW} - 6\pi a\mu_0\lambda(u - u_D), \tag{3.1}$$

where $u_D = -Dc^{-1}(dc/dx)$ is the vesicle diffusion velocity based on Fick's law and u is the actual velocity of the vesicle. One notes that as F_{VW} approaches zero u approaches u_D.

The two key quantities in (3.1) that need to be determined are the hydrodynamic interaction parameter λ and the macroscopic London–van der Waals attractive force F_{VW} between the vesicle and the plasmalemma. For present purposes it is reasonable to neglect the deformations of the vesicle and plasmalemma membranes and to derive approximate expressions for both λ and F_{VW} treating the vesicle approach as that of a spherical particle interacting with a planar boundary. For this simpler geometry, Cox & Brenner (1968) have developed an exact series solution for the quasi-steady-state Stokes drag on a

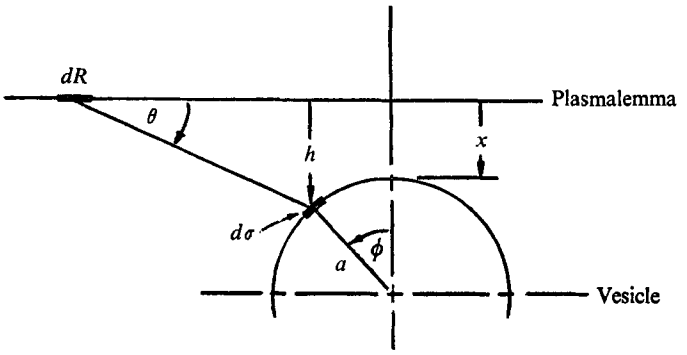

FIGURE 4. Sketch showing geometry and co-ordinates for evaluation of the van der Waals force integral, equations (3.4) and (3.5).

$1+\frac{x}{a}$	λ exact equation (3.2)	λ approx. equation (3.3)
1·020	51·594	51·00
1·127	9·252	8·874
1·543	3·036	2·842
2·352	1·837	1·739
3·762	1·413	1·362
6·132	1·222	1·195
10·06	1·125	1·110

TABLE 1. Comparison of approximate (3.3) and exact (3.2) (Cox & Brenner 1968) expressions for the Stokes correction factor λ for normal approach of a spherical particle to a planar boundary.

spherical particle of radius a as a function of the fluid gap x between the particle and the boundary; see figure 4. The expression for λ derived from this result is

$$\left.\begin{aligned}\lambda &= \tfrac{4}{3}\sinh\alpha \sum_{n=1}^{\infty} \frac{n(n+1)}{(2n-1)(2n+3)}\left[\frac{2\sinh(2n+1)\alpha+(2n+1)\sinh 2\alpha}{4\sinh^2(n+\tfrac{1}{2})\alpha-(2n+1)^2\sinh^2\alpha}-1\right],\\ \alpha &= \cosh^{-1}[(x+a)/a].\end{aligned}\right\} \quad (3.2)$$

Expression (3.2) is still too complicated to use in the present analysis and obtain closed-form solutions. A surprisingly close approximation to this exact solution which greatly simplifies the analysis is given by the much simpler expression

$$\lambda = 1+a/x. \quad (3.3)$$

Expression (3.3) approaches the Taylor lubrication formula as the gap width x goes to zero and the result for an isolated single sphere as x becomes large. A comparison between the approximate (3.3) and exact (3.2) expression for λ is shown in table 1, where it may be seen that the maximum deviation for any value of x/a is about 5 %.

A rigorous derivation of an expression for F_{VW} should take into account both the gradual shift with distance between the r^{-6} and r^{-7} behaviour characterizing respectively the non-retarded and retarded induced dipole molecular interaction

potential, and molecular interference effects arising from multiparticle interactions. This sophistication is well beyond the scope of the present treatment, which is based on the Lifshitz (1956) theory for binary molecular interactions and the idealized geometry shown in figure 4. The model further assumes that the molecules in the vesicle and plasmalemma membrane are concentrated at their respective surfaces and that only the molecules on the forward half of the vesicle adjacent to the plasmalemma contribute to the integrated macroscopic force.

The force dF_{VW} on a differential area element of the vesicle surface $d\sigma$ due to a non-retarded binary interaction potential integrated over all molecules at the plasmalemma surface is

$$dF_{VW} = \int_0^\infty \frac{k \sin\theta (2\pi R)\, d\sigma}{(R^2+h^2)^{\frac{7}{2}}}\, dR = \frac{3\pi k\, d\sigma}{h^5}. \tag{3.4}$$

Here h is the normal distance of the area element $d\sigma$ from the plasmalemma, R is the radial distance from this normal and k is a constant which is proportional to the surface density of molecules and the polarization properties of phospholipid bilayer membranes. Summing the differential force over the entire frontal portion of the vesicle one has

$$F_{VW} = 6\pi^2 a^2 k \int_0^{\frac{1}{2}\pi} \frac{\sin\phi\, d\phi}{[x+a(1-\cos\phi)]^5}, \tag{3.5}$$

where the denominator of the integral is the distance h defined by the geometry in figure 4. The evaluation of the integral in (3.5) is straightforward:

$$F_{VW} = \tfrac{3}{2}\pi^2 k[x^{-4} - (x+a)^{-4}]. \tag{3.6}$$

Combining results (3.3) and (3.6) and substituting in (3.1) yields

$$0 = \tfrac{3}{2}\pi^2 ka[x^{-4} - (x+a)^{-4}] - 6\pi\alpha\mu_0(1+a/x)\,(u-u_D). \tag{3.7}$$

The constant k in (3.7), which is related to Hamaker's constant, can be expressed in terms of fundamental membrane properties. However, these properties are difficult to measure experimentally. Instead of treating the constant k as an unknown free parameter in the theory it is more convenient to use k to define the characteristic length scale ϵ_0 for the London–van der Waals force interaction and then consider ϵ_0 as the free parameter in the theory. One observes from (3.7) that when $u = 2u_D$ the London–van der Waals and concentration-gradient driving forces will be exactly equal. This distance $x = \epsilon_0$ thus provides a convenient definition of the characteristic reference length for the vesicle motion near the plasmalemma. This definition of ϵ_0 leads to the following expression for k:

$$k = \frac{4a\mu_0 u_D}{\pi}\left[\frac{\epsilon_0^3(a+\epsilon_0)^5}{(a+\epsilon_0)^4 - \epsilon_0^4}\right]. \tag{3.8}$$

Finally, substituting (3.8) in (3.7) and simplifying, one obtains the desired result, an expression for the ratio of the actual approach velocity u of the vesicle to the

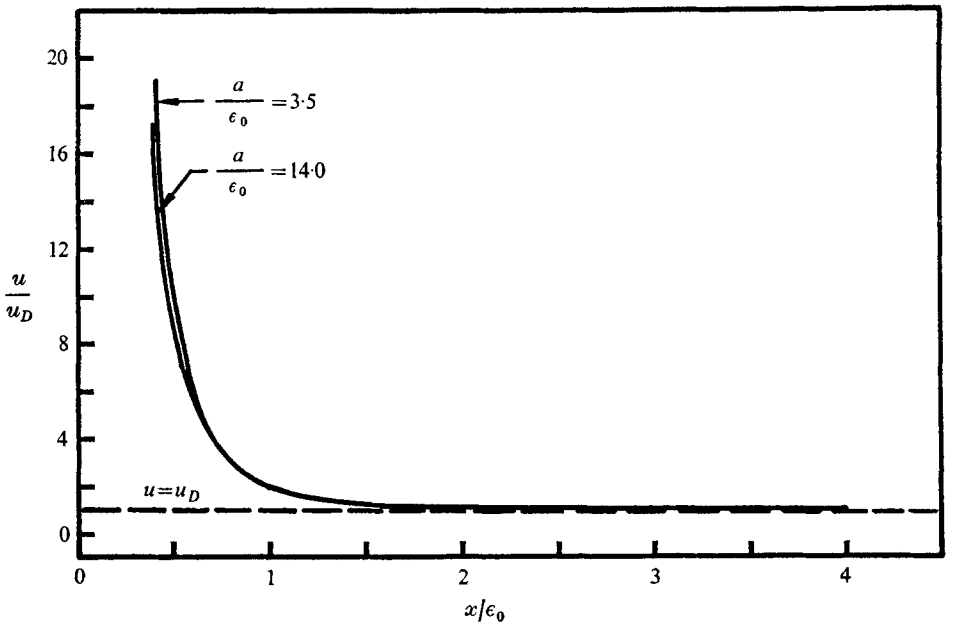

FIGURE 5. Increase in vesicle migration velocity due to van der Waals attractive forces as a function of dimensionless gap width x/ϵ_0 between vesicle and plasmalemma membrane. u_D = diffusion velocity in absence of London–van der Waals forces. Theoretical curves based on equation (3.9). a = 350 Å.

diffusion velocity u_D as a function of the dimensionless fluid gap x/ϵ_0 and vesicle radius a/ϵ_0:

$$\frac{u}{u_D} = 1 + \left(\frac{\epsilon_0}{x}\right)^3 \left(\frac{1+\frac{a}{\epsilon_0}}{\frac{x}{\epsilon_0}+\frac{a}{\epsilon_0}}\right)^5 \left[\frac{\left(\frac{a}{\epsilon_0}+\frac{x}{\epsilon_0}\right)^4 - \left(\frac{x}{\epsilon_0}\right)^4}{\left(\frac{a}{\epsilon_0}+1\right)^4 - 1}\right]. \tag{3.9}$$

Figure 5 is a plot of (3.9) for two different values of a/ϵ_0 (ϵ_0 = 25 and 100 Å) which are near the upper and lower limits that one might expect to find in an nedothelial cell. It is evident from this figure that the vesicle velocity u increases very rapidly as the gap distance narrows and that this behaviour is relatively insensitive to a/ϵ_0, at least when $a/\epsilon_0 > 3{\cdot}5$. At $x/\epsilon_0 = 0{\cdot}5$ the vesicle velocity is already more than 8 times the diffusion velocity and increasing at a rate which is approximately proportional to $(\epsilon_0/x)^3$, whereas at $x/\epsilon_0 \geqslant 2{\cdot}0$, u is essentially equal to u_D. This behaviour is, of course, a reasonable explanation of why vesicles are seldom seen in the process of reattaching. When $a/\epsilon_0 \gg 1$ equation (3.9) can be approximated by the much simpler equation

$$u \approx u_D[1 + (\epsilon_0/x)^3]. \tag{3.10}$$

3.2. *Vesicle density profile near plasmalemma*

The approximate expression for u given by (3.10) can be used to derive a simple closed-form relation which shows the effect of the London–van der Waals force on the vesicle density distribution near the plasmalemma. In the steady state,

the conservation equation for the vesicle number density c can be described by a continuum equation of the form

$$\frac{d}{dx}(cu_{VW}) = \frac{d}{dx}\left(D(x)\frac{dc}{dx}\right), \tag{3.11}$$

where u_{VW} can be thought of as a convective velocity for the vesicles created by the macroscopic London–van der Waals force and D is a spatially varying diffusion coefficient which takes account of the increased hydrodynamic resistance of the vesicle as it approaches the plasmalemma. The continuum hypothesis is justified although the vesicle dimensions are of the same order as the characteristic near-field diffusion distance ϵ_0 since $x_e/\epsilon_0 \ll 1$, where x_e is the amplitude of the individual random thermal excursions defined in (2.6).

The total velocity u which appears in (3.9) or (3.10) is the sum of u_{VW} and the vesicle diffusion velocity u_D. The integral of (3.11) therefore states that in the steady state the total vesicle flux is a constant, i.e.

$$cu = -A, \tag{3.12}$$

where A is a positive constant since u is in the $-x$ direction. Combining (3.10) and (3.12) one obtains

$$\frac{dc}{dx} = \frac{A}{D(x)}\left[\frac{(x/\epsilon_0)^3}{1+(x/\epsilon_0)^3}\right]. \tag{3.13}$$

In order that the Stokes–Einstein relation for the diffusion coefficient

$$D = \kappa R/6\pi\mu a, \tag{3.14}$$

which is valid for a dilute system of particles in an infinite medium, may be applied to the present flow configuration one must modify μ to reflect the hydrodynamic interaction between the vesicle and the plasmalemma. We thus treat μ in (3.14) as an effective viscosity coefficient defined by

$$\mu = \lambda\mu_0, \tag{3.15}$$

where μ_0 is the actual fluid viscosity and λ is the hydrodynamic interaction parameter [see (3.2) or (3.3)], which corrects the Stokes frictional resistance on an isolated sphere to that on a spherical vesicle whose flow geometry is shown in figure 4. From (3.14) and (3.15) a suitable approximation for $D(x)$ is

$$D(x) = D_0/\lambda(x), \tag{3.16}$$

where D_0 is the vesicle diffusion coefficient in an infinite medium.

When $a/x \gg 1$, $\lambda(x)$ from (3.3) is approximately equal to a/x and $D(x) \approx D_0(x/a)$. Inserting this expression for $D(x)$ in (3.13) and integrating leads to the result

$$cD_0/aA = \tfrac{1}{3}\ln[1+(x/\epsilon_0)^3] + b_1. \tag{3.17a}$$

The constant A in (3.17a) is still unknown, but is determined by matching the behaviour of the solution (3.17a) for $x/\epsilon_0 \gg 1$ with the large-scale solution for the

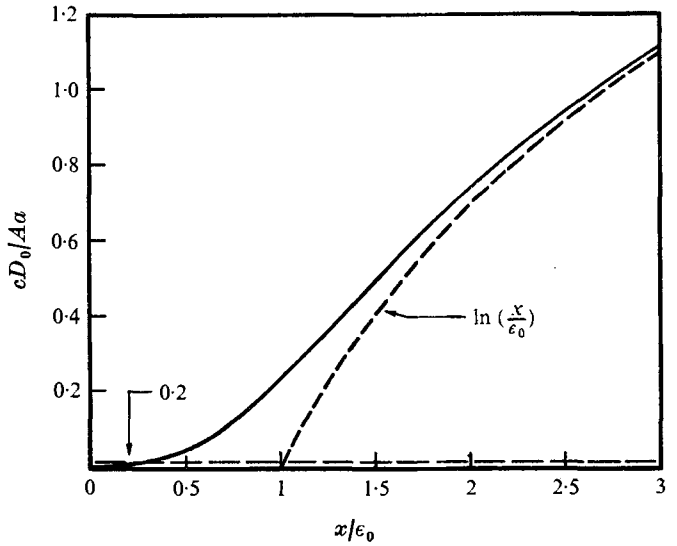

FIGURE 6. Dimensionless concentration profile near plasmalemma. Solid curve, equation (3.17*a*) with $b_1 = 0$; dashed curve, limiting behaviour of equation (3.17*b*) for $x/\epsilon_0 \gg 1$ and $x_1/\epsilon_0 = 0$; horizontal broken line, abscissa for $x_1/\epsilon_0 = 0{\cdot}2$.

vesicle density distribution in the interior of the cell. The constant of integration b_1 is determined by requiring the free-vesicle concentration to vanish at the distance of closest approach x_1/ϵ_0 of the vesicle to the plasmalemma before reattachment. Substituting this value of b_1 back into (3.17*a*) leads to

$$\frac{cD_0}{aA} = \tfrac{1}{3}\ln\left[\frac{1+(x/\epsilon_0)^3}{1+(x_1/\epsilon_0)^3}\right]. \tag{3.17b}$$

In figure 6 we have plotted (3.17*b*) with $x_1/\epsilon_0 = 0$. The dashed curve in this figure is the asymptotic behaviour of (3.17*b*) for $x/\epsilon_0 \gg 1$ extrapolated back to the abscissa. This is the behaviour that would occur if the London–van der Waals forces were neglected and thus represents the continuation of the solution curve for the vesicle density profile in the interior of the cell to the $c = 0$ axis when $x_1/\epsilon_0 = 0$. For other values of x_1/ϵ_0 the $c = 0$ axis is simply shifted upwards till it intersects the solid curve at the desired value of x_1/ϵ_0. The broken horizontal line in figure 6 represents such a shift for the case $x_1/\epsilon_0 = 0{\cdot}2$. The effective inward displacement Δx of the boundary as seen by the solution in the cell interior for any value of x_1/ϵ_0 is given by

$$\Delta x = \epsilon_0[1+(x_1/\epsilon_0)^3]^{\frac{1}{3}}. \tag{3.18}$$

The dimensionless distance $\epsilon = \Delta x/l$, which plays the same role as a displacement thickness in fluid boundary-layer theory, will be defined as the London–van der Waals force cut-off distance for the large-scale solution in the cell interior.

3.3. *Vesicle diffusion in the cell interior*

The continuum equation describing the steady-state diffusion in the cell interior of vesicles released at the luminal surface is

$$\frac{d}{dx}\left(D\frac{dc}{dx}\right) = 0, \quad \epsilon \leqslant x \leqslant y^-, \quad y^+ \leqslant x \leqslant 1-\epsilon, \tag{3.19}$$

where $D(x)$ is a spatially varying diffusion coefficient which considers the hydrodynamic interaction with both boundaries and x is a normalized co-ordinate which is scaled relative to the actual diffusion distance l between the plasmalemmas, which for the dimensions shown in figure 2 is approximately 2500 Å. The region of validity of (3.19) excludes the vesicle release point $x = y$ and the small regions $0 \leqslant x \leqslant \epsilon$ and $1-\epsilon \leqslant x \leqslant 1$ near each plasmalemma, which are defined by the apparent-boundary concept or effective London–van der Waals cut-off distance described in § 3.2. Thus, as shown in figure 6, we require that the free-vesicle density vanish at a distance ϵ from each boundary, i.e.

$$c(\epsilon) = 0, \quad c(1-\epsilon) = 0. \tag{3.20}$$

The special treatment of these small regions is important even though $\epsilon \ll 1$ since the hydrodynamic resistance is rapidly varying as one approaches the edges of the cell.

At $x = y$, the average intrusion distance for vesicles released from the luminal membrane, the concentration of free vesicles is continuous,

$$c(y^-) = c(y^+), \tag{3.21}$$

but there is a discontinuity in concentration gradient given by

$$\phi = D\left(\frac{dc}{dx}(y^-) - \frac{dc}{dx}(y^+)\right). \tag{3.22}$$

Here $\phi = N_a/t_a$ is the vesicle release rate per unit area of luminal surface and N_a is the number density of attached vesicles. Equation (3.19) is also valid in the range $\epsilon \leqslant x < 1-y$ and $1-y < x \leqslant 1-\epsilon$ for vesicles released at the abluminal surface, where at $x = 1-y$ equivalent matching conditions to (3.21) and (3.22) hold. Statistical studies performed by Bruns & Palade (1968) and Casley-Smith (1969) for the number-density profile of free vesicles in the cell interior and attached vesicles at each plasmalemma show that the vesicle transport is nearly symmetric.

In accord with our previous approximation for λ, equation (3.3) for the perpendicular motion of a spherical vesicle near a planar boundary, we shall approximate λ for the normal motion between two parallel walls by

$$\lambda(x) = 1 + \frac{a}{x} + \frac{a}{1-x}. \tag{3.23}$$

Using this approximation for λ in (3.17) and substituting the resulting expression for $D(x)$ in (3.19) one obtains

$$\frac{d}{dx}\left(\frac{x(1-x)}{a+x(1-x)}\frac{dc}{dx}\right) = 0. \tag{3.24}$$

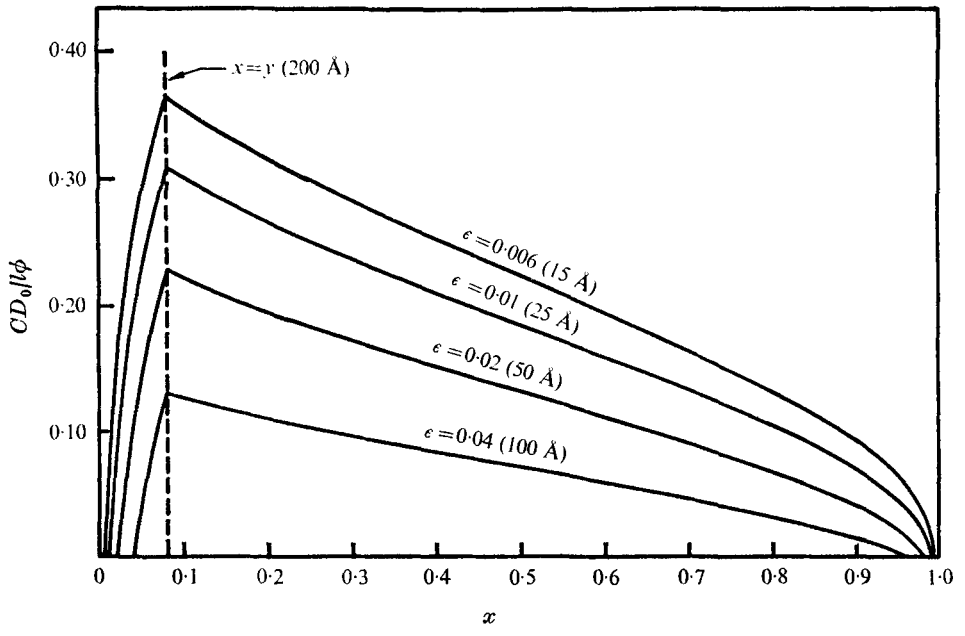

FIGURE 7. Theoretical solution for dimensionless steady-state concentration distribution of free vesicles released at luminal membrane for representative values of the effective van der Waals cut-off distance ϵ based on equations (3.25*a*) and (3.25*b*).

The solution to (3.24) which satisfies the boundary and matching conditions (3.21)–(3.23) is

$$c(x) = \begin{cases} \dfrac{l\phi}{D_0} F(a,y,\epsilon)\left[x-\epsilon+a\ln\dfrac{x(1-\epsilon)}{\epsilon(1-x)}\right], & \epsilon \leqslant x \leqslant y, \quad (3.25a) \\ \dfrac{l\phi}{D_0}(F(a,y,\epsilon)^{-1})\left[x+\epsilon-1+a\ln\dfrac{x\epsilon}{(1-x)(1-\epsilon)}\right], & y < x \leqslant 1-\epsilon, \quad (3.25b) \end{cases}$$

where $F(a,y,\epsilon)$ is an interaction function which depends only on the geometry of the flow configuration and the effective London–van der Waals cut-off distance:

$$F(a,y,\epsilon) = \frac{y+\epsilon-1+a\ln[y\epsilon/(1-y)(1-\epsilon)]}{2\epsilon-1+2a\ln[\epsilon/(1-\epsilon)]}. \quad (3.26)$$

The unknown constant A in the solution for the vesicle density distribution near the plasmalemma can now be determined by matching the behaviour of (3.17) for large values of x/ϵ_0 with the behaviour of (3.25*a*) as x approaches ϵ. The value of A determined in this manner is

$$A = l\phi F(a,y,\epsilon). \quad (3.27)$$

The dimensionless concentration profile given by (3.25) is plotted in figure 7 for four representative values of ϵ. It is evident from this figure that the smaller the value of ϵ the larger the concentration gradient of vesicles in the vicinity of the plasmalemma membrane and the larger the total free-vesicle population (the area under the concentration curve) for a fixed source strength ϕ. In

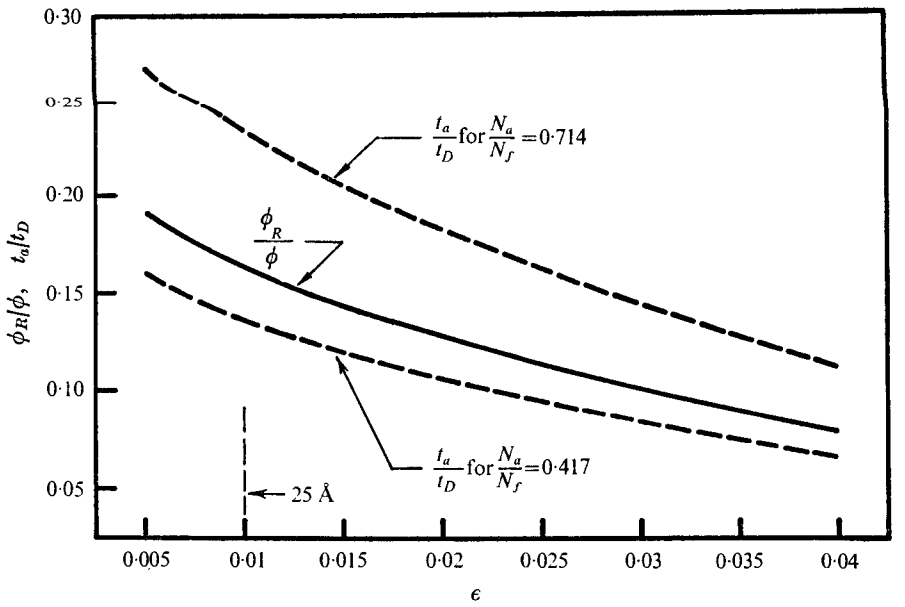

FIGURE 8. Theoretical solution for the fractional flux ϕ_R/ϕ of vesicles crossing the cell and the ratio t_a/t_D of vesicle attachment to diffusion times as a function of ϵ based on equations (3.28*b*) and (3.29).

essence, the more closely the vesicle can approach the plasmalemma before coming under the influence of strong London–van der Waals forces of attraction the greater the retarding effect of the viscous resistance in the narrowing fluid gap between the vesicle and the wall. The concentration profile which bears the closest qualitative resemblance to the steady-state vesicle concentration profiles observed by Casley-Smith & Chin (1971) in their electron microscopic studies is the solution for $\epsilon = 0{\cdot}006$. This corresponds to a cut-off distance of about 15 Å.

One can show from (3.22) and (3.25) that the fraction ϕ_L/ϕ of the vesicles released that return to the luminal membrane and the fraction ϕ_R/ϕ that are transported across the cell are given by

$$\phi_L/\phi = F(a, y, \epsilon), \quad \phi_R/\phi = 1 - F(a, y, \epsilon). \tag{3.28a,b}$$

Results (3.28*a*, *b*) are more conveniently written in terms of t_a, t_D and the density N_f of free and the density N_a of attached vesicles per unit area of endothelial surface. Assuming that the transport across the cell is symmetric, $\phi_R = N_f/2t_D$, where the factor $\frac{1}{2}$ enters ϕ_R since only half the free vesicles are diffusing towards the abluminal surface. Inserting these expressions into (3.28) one finds

$$t_a/t_D = 2(N_a/N_f)(1 - F(a, y, \epsilon)). \tag{3.29}$$

The vesicle number flux ϕ_R per unit area across the endothelial cell layer can be conveniently written in terms of the total vesicle population N per unit area of endothelial surface. From (3.28), (3.29) and the definition $N \equiv 2N_a + N_f$,

$$\phi_R = N(1-F)/2[t_a + t_D(1-F)]. \tag{3.30}$$

In figure 8 we have plotted the theoretical predictions of (3.28) and (3.29) for the variations of ϕ_R/ϕ and t_a/t_D as a function of ϵ. The actual counted values of N_a and N_f given in Casley-Smith (1969) vary somewhat between different endothelial cells, with the result that N_a/N_f lies in the range $0{\cdot}417 < N_a/N_f < 0{\cdot}714$. The dashed curves for t_a/t_D in figure 8 correspond to these lower and upper limits respectively. If Δx in (3.18) is 15 Å this means that t_a is somewhere between 0·15 and 0·29 of t_D. The ratio t_a/t_D is proportional to ϕ_R/ϕ and in general decreases as ϵ increases for a fixed value of N_a/N_f. This behaviour as a function of ϵ is expected since the likelihood that a vesicle will not reattach at the same surface from which it was released and hence cross the cell increases the further ϵ is removed from the release point $x = y$.

The dimensionless concentration $cD_0/\phi l$ and the flux ratios ϕ_L/ϕ and ϕ_R/ϕ are all independent of the intracellular viscosity μ_0. This is an important result since as noted previously there is considerable uncertainty in the actual value of μ_0 and hence D_0. On the other hand, the absolute value of the transendothelial flux ϕ_R and the ratio of t_a/t_D do depend on μ_0 since the vesicle population ratio N_a/N_f is a function of μ_0.

The two key results of this section are (3.29) and (3.30) for the ratio t_a/t_D and the vesicle number flux ϕ_R. For the reasons stated in the introduction direct observational estimates of t_D are at present unreliable. The principal quantitative applications of the theory for the moment are the time-dependent uptake experiments with albumin and other labelled macromolecules, using the composite diffusion model for the arterial wall developed in the next section. Equation (3.30) will be used to construct the interface boundary condition (4.3) for this model, while (3.29) will be used in the derivation of the new expression (4.32) for the vesicle diffusion time t_D.

4. Composite diffusion model for the arterial wall

We should now like to incorporate the solution for the vesicle number flux ϕ_R given by (3.30) into an overall transient diffusion model for the arterial wall. Figure 9 is a diagrammatic sketch of this proposed model based on the electron micrograph figure 1(*a*). For dog common carotid artery the inner endothelial lining is approximately 0·0005 of the total wall thickness. In our simplified mathematical model the endothelium is treated as a vanishingly thin layer located at the origin of a one-dimensional co-ordinate system and the smooth muscle cells in the underlying tissue as a uniformly distributed array of identical cells.

The dimensionless partial differential equations governing the one-dimensional transient diffusion of macromolecules in the interstitial and intracellular phases are

$$\alpha_1 \frac{\partial C_1}{\partial \tau} - \frac{\partial^2 C_1}{\partial X^2} = \beta(C_2 - C_1), \tag{4.1}$$

$$\alpha_2 \partial C_2/\partial \tau = \beta(C_1 - C_2). \tag{4.2}$$

Here C_1 and C_2 are the dimensionless concentrations in the interstitial and

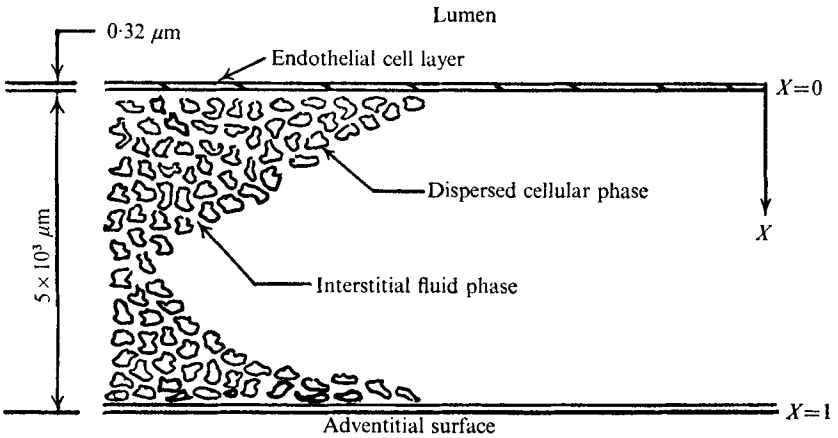

FIGURE 9. Schematic illustration for two-phase mathematical model of the arterial wall for transient diffusion and uptake of macromolecules. Dimensions based on canine carotid artery.

dispersed cellular phases, respectively, scaled relative to the concentration c_p in the arterial lumen, α_i is the volume fraction occupied by each phase, τ and X are dimensionless time and distance co-ordinates, $\tau = tD_m/L^2$ and $X = x/L$, where D_m is the macromolecule diffusion coefficient in the interstitial fluid, and β is a dimensionless number defined by $\beta = PL^2/D_m$, where P is a membrane permeability coefficient for the molecular diffusion of the macromolecules into the dispersed cellular phase. A plausible membrane molecular structure which facilitates this diffusion is described in the fluid mosaic model of Singer & Nicolson (1972). Thus β represents the ratio of the membrane diffusion flux into the dispersed cellular phase to the molecular diffusion flux in the interstitial fluid. The right-hand side of (4.1) describes a uniformly distributed continuum of point sinks whose strength is proportional to the local concentration difference between the two phases. Equation (4.2) for the dispersed cellular phase assumes that vesicular transport and membrane molecular diffusion across the smooth muscle cells do not contribute significantly to the total macromolecule transport across the wall and that the time constant for the equilibration of the intracellular contents is short compared with the interstitial fluid diffusion time. These conditions are satisfied for large arteries where the dimensions of the muscle cells are small compared with the wall thickness. This mathematical description is consistent with the ultrastructural specialization discussed at the end of the introduction.

The important feature of the present boundary-value problem which differentiates it from the heterogeneous tissue model developed by Hills (1968, 1970) is the vesicular transport boundary condition imposed by the thin surface layer of endothelial cells.† If c_p and $c(0)$ are the dimensional macromolecule concentrations at the luminal and abluminal surfaces of the endothelial cell layer respectively and V is the internal volume of the vesicles, then the net macromolecule

† The authors were unaware of Hills's model when the present theory was developed and would like to thank M. J. Lever for first bringing it to their attention.

flux across the endothelium due to the vesicle transport is $\phi_R V(c_p - c(0))$, where ϕ_R, the transendothelial vesicle number flux in either direction, is given by (3.30). If the macromolecule flux down the intercellular clefts and filtration flow in the interstitial fluid are both assumed negligible, then this net vesicle flux must be equal to the molecular diffusive flux at the abluminal tissue interface. The non-dimensional boundary condition at $x = 0$, the interface, is thus

$$-\partial C_1/\partial X = \sigma(1 - C_1(0)), \tag{4.3}$$

where $\sigma = \phi_R VL/D_m$ is a dimensionless number characterizing the vesicular transport. For an injured artery whose endothelium has been removed (4.3) is replaced at $X = 0$ by

$$C_1(0) = 1. \tag{4.4}$$

Boundary condition (4.3) is analogous to that for a high resistance film in heat-transfer problems.

The usual boundary condition at $X = 1$, the adventitial surface, for *in vitro* experiments is

$$C_1(1) = 0. \tag{4.5}$$

This corresponds to a dilute, well-mixed outer bathing solution. The usual initial conditions for an *in vitro* experiment are

$$C_1(x, 0) = C_2(x, 0) = 0. \tag{4.6}$$

4.1. *Solution for normal artery*

The boundary- and initial-value problem for a normal artery is defined by (4.1)–(4.3), (4.5) and (4.6). The solution for the interstitial fluid concentration C_1 is conveniently written as a linear superposition of a time-independent solution C_{s1} which satisfies the inhomogeneous boundary condition (4.3) and a transient solution $\tilde{C}_1$ which obeys homogeneous boundary conditions but inhomogeneous initial conditions. Thus we let

$$C_1(X, \tau) = \tilde{C}_1(X, \tau) + C_{s1}(X), \tag{4.7}$$

where C_{s1}, $\tilde{C}_1$ and C_2 satisfy the following equations and boundary and initial conditions derived from (4.1)–(4.6). For C_{s1} we have

$$d^2C_{s1}/dX^2 - \beta C_{s1} = 0, \tag{4.8}$$

$$-dC_{s1}/dX = \sigma(1 - C_{s1}(0)), \quad X = 0, \tag{4.9}$$

$$C_{s1} = 0, \quad X = 1. \tag{4.10}$$

For $\tilde{C}_1$ and C_2 we have

$$\alpha_1 \frac{\partial \tilde{C}_1}{\partial \tau} - \frac{\partial^2 \tilde{C}_1}{\partial X^2} = \beta(C_2 - \tilde{C}_1), \tag{4.11}$$

$$\alpha_2 \partial C_2/\partial \tau = \beta(\tilde{C}_1 - C_2) + \beta C_{s1}, \tag{4.12}$$

$$\partial \tilde{C}_1/\partial X + \sigma \tilde{C}_1 = 0, \quad X = 0, \tag{4.13}$$

$$\tilde{C}_1(1, \tau) = 0, \quad \tilde{C}_1(X, 0) = -C_{s1}(X), \quad C_2(X, 0) = 0. \tag{4.14)–(4.16}$$

The solution to (4.8) which satisfies boundary conditions (4.9) and (4.10) is given by

$$C_{s1}(x) = \frac{\sigma \sinh[\beta^{\frac{1}{2}}(1-X)]}{\sigma \sinh \beta^{\frac{1}{2}} - \beta^{\frac{1}{2}} \cosh \beta^{\frac{1}{2}}}. \tag{4.17}$$

Substituting (4.17) into (4.7), one assumes series solutions for C_1 and C_2 of the form

$$C_1(X,\tau) = \frac{\sigma \sinh[\beta^{\frac{1}{2}}(1-X)]}{\sigma \sinh \beta^{\frac{1}{2}} - \beta^{\frac{1}{2}} \cosh \beta^{\frac{1}{2}}} + \sum_{n=1}^{\infty} A_n(\tau) \sin \lambda_n (1-X), \tag{4.18}$$

$$C_2(X,\tau) = \sum_{n=1}^{\infty} B_n(\tau) \sin \lambda_n (1-X), \tag{4.19}$$

where $A_n(\tau)$ and $B_n(\tau)$ are unknown functions to be determined and the λ_n comprise an ordered series of eigenvalues which are derived from the homogeneous boundary conditions (4.13) and (4.14). These eigenvalues satisfy the algebraic relation

$$\tan \lambda_n = -\lambda_n/\sigma. \tag{4.20}$$

To determine $A_n(\tau)$ and $B_n(\tau)$ we first express the solution for C_{s1} given by (4.17) as a Fourier series in the fundamental eigenfunctions $\sin \lambda_n(1-X)$:

$$C_{s1}(X) = \sum_{n=1}^{\infty} a_n \sin \lambda_n (1-X), \tag{4.21}$$

where the evaluation of the coefficients a_n is tedious but straightforward. The final result is

$$a_n = \frac{4\sigma\lambda_n^2 \sin \lambda_n}{(\beta+\lambda_n^2)(2\lambda_n - \sin 2\lambda_n)}. \tag{4.21a}$$

By substituting the infinite series representations (4.18), (4.19) and (4.21) into (4.11) and (4.12), one obtains the following differential equations for the A_n and B_n:

$$\alpha_1 dA_n/d\tau + \lambda_n^2 A_n = \beta(B_n - A_n), \tag{4.22}$$

$$\alpha_2 dB_n/d\tau + \beta(B_n - A_n) = \beta a_n. \tag{4.23}$$

The solutions of (4.22) and (4.23) which satisfy the initial conditions (4.15) and (4.16) are

$$A_n(\tau) = A_{n1}(e^{k_{n1}\tau} - e^{k_{n2}\tau}) + \frac{\alpha_n}{\lambda_n^2}[\beta - (\beta+\lambda_n^2)e^{k_{n2}\tau}], \tag{4.24}$$

$$B_n(\tau) = \frac{A_{n1}\beta}{\alpha_2 k_{n1} + \beta}(e^{k_{n1}\tau} - e^{k_{n2}\tau}) + \frac{a_n}{\lambda_n^2}(\beta+\lambda_n^2)(1 - e^{k_{n2}\tau}), \tag{4.25}$$

where

$$A_{n1} = a_n k_{n2} \left(\frac{\beta+\lambda_n^2}{\beta\lambda_n^2}\right)\left(\frac{\alpha_2 k_{n1} + \beta}{k_{n1} - k_{n2}}\right), \tag{4.26}$$

$$k_{ni} = -\frac{1}{2}\left(\frac{\lambda_n^2}{\alpha_1} + \frac{\beta(\alpha_1+\alpha_2)}{\alpha_1\alpha_2}\right) \pm \frac{1}{2}\left[\left(\frac{\lambda_n^2}{\alpha_1} + \frac{\beta(\alpha_1+\alpha_2)}{\alpha_1\alpha_2}\right)^2 - \frac{4\beta\lambda_n^2}{\alpha_1\alpha_2}\right]^{\frac{1}{2}}. \tag{4.27}$$

The exponential decay constants k_{n1} and k_{n2} correspond to the plus and minus signs in (4.27) respectively. This completes the solution for the unknown functions $A_n(\tau)$ and $B_n(\tau)$ in the series solutions (4.18) and (4.19) for the concentrations C_1 and C_2 in the interstitial fluid and dispersed cellular phase respectively.

For very large times the solutions for C_1 and C_2 approach an asymptotic behaviour that is independent of τ. This asymptotic solution

$$C_1(X,\infty) = C_2(X,\infty) = \frac{\sigma}{1+\sigma}(1-X) \tag{4.28}$$

reveals that in the steady state the interface concentration is given by $\sigma/(1+\sigma)$. The ratio of the resistances R_e and R_w offered by the endothelium and the arterial wall in the steady state is simply the ratio of the concentration drop across the endothelium to that across the rest of the arterial wall. From (4.28)

$$R_e/R_w = 1/\sigma. \tag{4.29}$$

The integrated uptake of labelled macromolecules present in the artery wall at time τ is

$$M = \alpha_1 \int_0^1 C_1(X,\tau)\,dX + \alpha_2 \int_0^1 C_2(X,\tau)\,dX. \tag{4.30}$$

The integrals in (4.30) are given by

$$\int_0^1 C_1(X,\tau)\,dX = \frac{\sigma(\cosh\beta^{\frac{1}{2}}-1)}{\sigma\beta^{\frac{1}{2}}\sinh\beta^{\frac{1}{2}} - \beta\cosh\beta^{\frac{1}{2}}} + \sum_{n=1}^{\infty}\frac{A_n(\tau)}{\lambda_n}(1-\cos\lambda_n), \tag{4.31a}$$

$$\int_0^1 C_2(X,\tau)\,dX = \sum_{n=1}^{\infty}\frac{B_n(\tau)}{\lambda_n}(1-\cos\lambda_n), \tag{4.31b}$$

where $A_n(\tau)$ and $B_n(\tau)$ are the coefficients (4.24) and (4.25).

The two unknown parameters σ and β which appear in the solution for the integrated uptake, (4.30) and (4.31), need to be determined experimentally. The parameter β will be determined by curve fitting the theoretical and experimental uptake curves for an injured artery in which the endothelium has been removed. These solutions, which are presented next, are independent of σ since the vesicle flux boundary condition (4.3) is replaced by boundary condition (4.4). The value of σ is now determined by curve fitting the uptake data for a normal artery. This value of σ is one of the most important results of the present model since it can be used to obtain an improved estimate of the vesicle diffusion time t_D, which at the moment is known only to order-of-magnitude accuracy from time-dependent ultrastructural studies. Combining the definition $\sigma = \phi_R VL/D_m$, the solution (3.30) for the vesicle flux ϕ_R and expression (3.29) for the ratio t_a/t_D one obtains

$$t_D = \frac{NVL}{2\sigma D_m(1+2N_a/N_f)}. \tag{4.32}$$

Using currently available uptake measurements t_D can be estimated from (4.32) to within roughly a factor of two.

4.2. *Solution for injured artery*

The boundary- and initial-value problem for an injured artery whose endothelium has been removed is defined by (4.1), (4.2) and (4.4)–(4.6). The solution procedure parallels that just developed for a normal artery with intact endothelium. The

formulation of the boundary- and initial-value problems for C_{s1}, $\tilde{C}_1$ and C_2 differs only in that (4.9) is replaced by $C_s(0) = 1$ and (4.13) is replaced by the homogeneous condition $\tilde{C}_1(0,\tau) = 0$. We shall give only the final results.

The new series solutions for C_1 and C_2 are of the form

$$C_1(X,\tau) = \sum_{n=1}^{\infty} A_n(\tau)\sin\lambda_n X + \frac{\sinh[\beta^{\frac{1}{2}}(1-X)]}{\beta^{\frac{1}{2}}}, \tag{4.33}$$

$$C_2(X,\tau) = \sum_{n=1}^{\infty} B_n(\tau)\sin\lambda_n X, \tag{4.34}$$

where the λ_n are the eigenvalues

$$\lambda_n = n\pi, \quad n = 1, 2, \ldots, \infty. \tag{4.35}$$

The solutions for the coefficients $A_n(\tau)$ and $B_n(\tau)$ in (4.33) and (4.34) are again given by (4.24) and (4.25) except that the constants k_{ni}, a_n and A_{n1} are changed. The new decay constants k_{ni} are given by (4.27) with the eigenvalues for λ_n the ordered roots (4.35). The expression for the Fourier coefficient a_n in the infinite series representation of the second term in (4.33) is

$$a_n = \frac{\int_0^1 \sinh[\beta^{\frac{1}{2}}(1-X)]\sin(\lambda_n X)\,dX}{\sinh\beta^{\frac{1}{2}}\int_0^1 \sin^2(\lambda_n X)\,dX} = \frac{2n\pi}{\beta+n^2\pi^2}, \tag{4.36}$$

and the value of A_{n1} given by (4.26) is modified according to the above results.

The integrated uptake of labelled molecules by the arterial wall is given by (4.30), where the integrals of the concentration are now

$$\int_0^1 C_1(X,\tau)\,dX = \frac{\cosh\beta^{\frac{1}{2}}-1}{\beta^{\frac{1}{2}}\sinh\beta^{\frac{1}{2}}} + \sum_{n=1,3,5\ldots}^{\infty} \frac{2A_n(\tau)}{n\pi}, \tag{4.36a}$$

$$\int_0^1 C_2(X,\tau)\,dX = \sum_{n=1,3,5\ldots}^{\infty} \frac{2B_n(\tau)}{n\pi}. \tag{4.36b}$$

The above solutions for our model of a two-phase injured wall will be compared in the next section with the solutions for a homogeneous single-phase wall. The latter solutions, for $\beta = 0$, are given in Carslaw & Jaeger (1959):

$$C_1(X,\tau) = 1 - X - \sum_{n=1}^{\infty} \frac{2}{n\pi}\exp(-n^2\pi^2\tau/\alpha_1)\sin n\pi X, \tag{4.37}$$

$$M(\tau) = \frac{\alpha_1}{2} - \sum_{n=1,3,5\ldots}^{\infty} \frac{4\alpha_1}{(n\pi)^2}\exp(-n^2\pi\tau/\alpha_1). \tag{4.38}$$

Note that the volume fraction α_1 has been retained in (4.37) and (4.38) so that the comparisons can be drawn on the basis of equal volumes.

5. Numerical results and comparison with experiments

At the time of writing experimental data were not available to perform a detailed comparison with the concentration profiles for a normal and injured artery predicted by (4.21) and (4.22), and (4.33) and (4.34). Experimental data

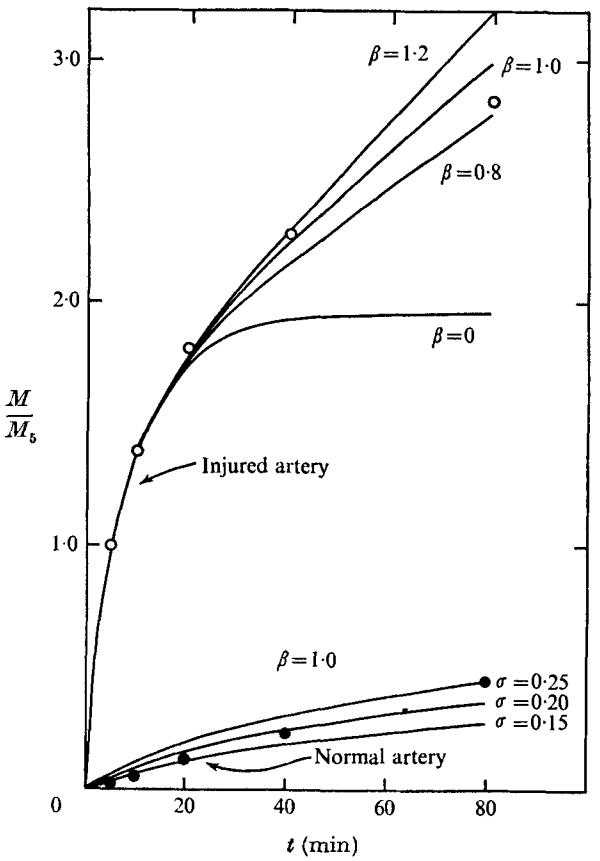

FIGURE 10. Comparison of theory and experiment (Fry 1973) for the time-dependent uptake of labelled albumin in normal and injured (endothelium removed) dog carotid artery. Values of M scaled relative to uptake in injured artery at $t = 5$ min. Theoretical curves based on equations (4.30) and (4.31) or (4.36).

do exist, however, for the time-dependent integrated uptake of a relatively inert macromolecule, labelled albumin, in excised preparations of dog common carotid artery using both radioactive tag (Caro *et al.* 1975) and Evans Blue dye (Fry 1973) techniques. These data have been used to estimate β, σ and the three characteristic diffusion times describing the vesicle transport across the endothelium and the macromolecule diffusion in each phase of the wall substance.

The procedure for determining β and σ described earlier is applied in figure 10 to Fry's experimental data for the time-dependent uptake of albumin, labelled with protein binding Evans Blues dye, in *in vitro* preparations of normal and injured canine carotid artery specimens. The injured preparations have had their endothelium removed by gentle stroking with a camel-hair brush. The theoretical uptake curves are given by (4.30) and (4.31) or (4.36) for the normal and injured artery respectively. The $\beta = 0$ solution curve is given by (4.38). All uptake results have been normalized by the integrated uptake M_5 in the injured wall at $t = 5$ min.

The theoretical curves for the injured wall provide an optimum fit with the

experimental data when $\beta = 1{\cdot}0$. One notes that, if there were no dispersed cellular phase (the $\beta = 0$ solution curve), the interstitial fluid pool would become saturated after about 40 min. The dispersed cellular phase is thus required to predict the more gradual increase in uptake characteristic of the larger time (t greater than roughly 30 min) experimental data.

For short times, t less than about 10 min, the effect of the long time intracellular capacitance and the finite dimensions of the wall are both negligible, and the artery wall with the endothelium removed exhibits the $t^{\frac{1}{2}}$ behaviour characteristic of a semi-infinite pure substance. Thus, for these short times the wall uptake is independent of β and determined only by the molecular diffusion coefficient D_m. The scaling of the dimensionless time τ in the theoretical solution is therefore conveniently determined by requiring exact numerical agreement between theory and experiment for all values of β at the first data point, $t = 5$ min. The dimensional reference time L^2/D_m established in this manner is $4{\cdot}0 \times 10^4$ s. If $L = 0{\cdot}5$ mm this yields $D_m = 6.25 \times 10^{-8}$ cm^2/s.† After 80 min, the longest duration of the experiment, the interstitial fluid pool is completely filled whereas the intracellular pool has filled to only about 7 % of its total capacitance, assuming a value for α_1 of 0·15. Using the value $\beta = 1{\cdot}0$ just determined, we plot the theoretical solution curves for the normal artery treating σ now as the free parameter. As observed in figure 10, a reasonably good fit of the experimental data is obtained for $\sigma = 0{\cdot}2$. The steady-state resistance to macromolecule transport of the thin layer of endothelial cells at the luminal surface is therefore, from (4.29), about five times that of the whole of the rest of the wall.

The three characteristic times describing the overall transport behaviour of the arterial wall can be estimated from the values of β and σ just determined and (4.32). In evaluating t_D from (4.32) we have used a value for N of 480 vesicles/μm^2 (Bruns & Palade 1968), a free-to-attached vesicle density ratio N_f/N_a of 2, an interior vesicle volume based on an internal radius $a_i = 275$ Å and the aforementioned values of L, σ and D_m. One finds that t_D is 8·3 s. Fry, in repeating the experiments shown in figure 10 with a doubly tagged albumin molecule, has observed that the initial rate of growth ($t < 10$ min) of the wall uptake in the wounded artery specimen, using the double tagging procedure, is substantially less than that shown in figure 10.‡ These new unpublished data suggest that the value of D_m calculated earlier is 2–3 times too large. A revised estimate of t_D using this corrected value for D_m in (4.32) is approximately 20 s. This downward correction for D_m is also consistent with the recent data of Caro *et al.* (1975) using I^{125} labelled albumin. The latter study indicates a roughly fourfold increase in the uptake of labelled albumin in the injured artery after 10 min rather than the more than tenfold increase noted in figure 10. The above estimate for t_D lies

† D_m is not the same as the average wall permeability coefficient P_w usually quoted in perfusion studies. The latter is defined as the number of counts per second per cm^2 of surface area of specimen divided by the time times the number of counts per cm^3/s of incubating fluid and has the units cm/s. P_w thus represents a diffusion coefficient per unit wall thickness. Correcting for the effective fractional area occupied by the interstitial space and dividing by the wall thickness one obtains $P_w = 3 \times 10^{-7}$ cm/s.

‡ Private communication.

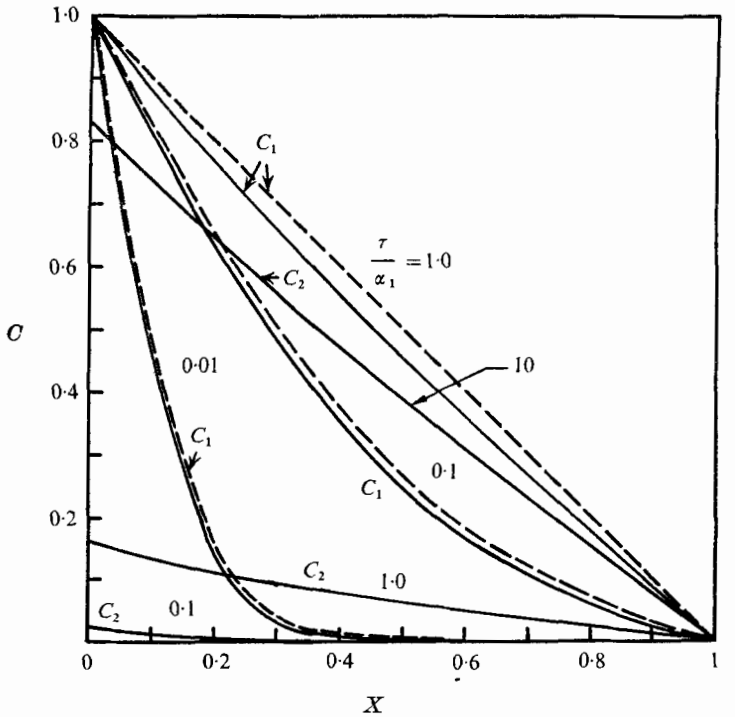

FIGURE 11. Comparison of theoretical concentration profiles in injured artery wall with (solid curves, $\beta = 1{\cdot}0$) and without (dashed curves, $\beta = 0$) dispersed cellular phase. C_1 = concentration in interstitial fluid, from equation (4.33) for $\beta = 1{\cdot}0$, from equation (4.37) for $\beta = 0$; C_2 = concentration in dispersed cellular phase, from equation (4.34).

between the 3–5 s estimate of Casley-Smith & Chin (1971) and the 45–60 s estimate of Simionescu *et al.* (1973) using observational electron microscopic tracer studies of mouse cardiac and rat capillary endothelium respectively. The characteristic reference time for the filling of the interstitial fluid pool is given by $\alpha_1 L^2/D_m$. Estimates for this time vary between approximately 30 min and $1\frac{1}{2}$ h depending on the value of D_m used. A rough estimate of the time required to fill the dispersed cellular phase can be obtained by continuing the $\beta = 1{\cdot}0$ solution curve to very large times. One finds that the intracellular phase is about 95 % filled after 72 h.

More detailed insight into the behaviour of the injured wall can be gained from the concentration profiles shown in figure 11. The dimensionless time $\tau/\alpha_1 = 0{\cdot}1$ corresponds to about 10 min in the real time co-ordinate plotted in figure 10. It is evident from figure 11 that the dispersed cellular phase acts as a continuously distributed sink which for the value $\beta = 1{\cdot}0$ has only a small effect on C_1. The maximum deviation occurs when τ/α_1 is $O(1)$. At this time C_1 has approached a quasi-steady-state distribution which is not quite linear because of the slow leakage into the intracellular phase, whereas C_2 is still far removed from its final steady-state distribution, which is achieved over a much longer time scale.

The dramatic differences in the time-dependent uptake of labelled albumin in injured and normal canine carotid artery observed in figure 10 can be explained

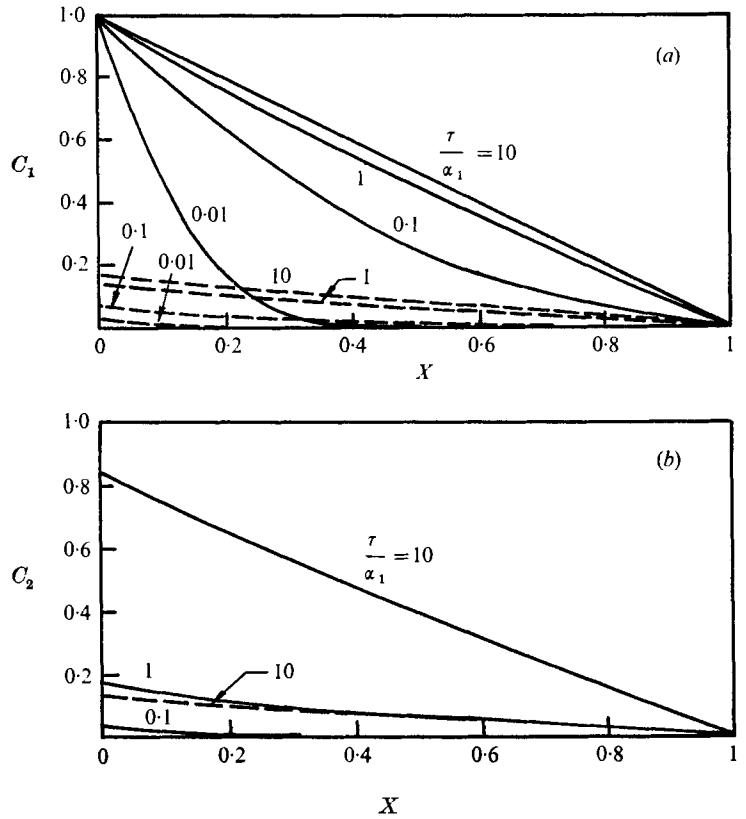

FIGURE 12. (*a*) Comparison of theoretical concentration profiles in interstitial fluid phase. – – –, normal artery wall, equation (4.18); ——, injured artery wall, equation (4.33). (*b*) Comparison of theoretical concentration profiles in dispersed cellular phase. – – –, normal artery wall, equation (4.19); ——, injured artery wall, equation (4.34). $\beta = 1{\cdot}0$, $\sigma = 0{\cdot}2$.

with the aid of the concentration profiles shown in figure 12. The striking difference between the two sets of curves is the greatly reduced level of the concentration $C(0)$ at the abluminal interface in the normal artery. For $\tau/\alpha_1 < 0{\cdot}1$ the area under the C_1 curve for the normal artery increases nearly linearly with time since from (4.3) the macromolecule flux across the interface is nearly constant and whatever enters is almost completely stored in the interstitial fluid pool. For intermediate times the finite thickness of the wall becomes important as well as the capacitance of the intracellular phase. The flux across the interface does not change substantially since the dimensionless concentration difference $1 - C(0)$ across the endothelium in (4.3) varies between 1 and 0·83, its steady-state value for $\sigma = 0{\cdot}2$; see (4.28). This flux is partially absorbed by both phases of the wall capacitance and partially transitted across the wall, where it is lost to the surrounding environment.

6. Concluding remarks

The principal objective of the present investigation has been to develop a plausible mathematical model for the transport of relatively inert macromolecules in the arterial wall under static *in vitro* conditions which considers the highly specialized ultrastructural function of the arterial endothelium and underlying tissue. This model is intended to provide the framework for more detailed theoretical and experimental studies in which the chemical kinetics of degradable macromolecules are important and various mechanical disturbances are introduced such as flow, pressure oscillations and periodic mechanical stretch. All these complications are, of course, present *in situ*. The initial experiments performed by the authors reported in Caro *et al.* (1974) strongly suggest that mechanical disturbances have an important influence on the uptake of macromolecules by the wall owing to the hydrodynamic interaction between the vesicles and the deformation of the endothelial cells produced by the mechanical disturbances.

A number of important new problems in mechanics have been identified, such as the equilibrium force balance that determines the size and shape of the attached and free vesicles, the nature of the instability that leads to the rupture of the vesicle stalks, the proper treatment of the London–van der Waals force interaction between the vesicle and the deforming plasmalemma boundaries of the cell, and the generalization of the vesicle diffusion equation which allows these forces to be taken into account. For the unsteady mechanical disturbances mentioned above, one is especially interested in the nature of the intracellular fluid currents that are generated by the deformation of the endothelial cell and the importance of viscoelastic behaviour of both the endothelial membrane and the intracellular contents. The fundamental processes that cause the enhanced vesicle transport when unsteady mechanical disturbances are present constitute an important area for new research.

The authors wish to express their gratitude to C. T. Lewis, G. E. Palade and M. and N. Simionescu for their valuable contributions to the electron microscopic aspects of the present theoretical study, M. J. Lighthill, K. Parker and T. Pedley for many helpful technical comments and R. Oxenham for all the computational results. The investigation was supported in part by the Medical Research Council and British Heart Foundation. S. Weinbaum was a Senior Visiting Fellow of the Scientific Research Council for the academic year 1973–1974, during which this work was initiated.

REFERENCES

Adams, C. W. M., Morgan, R. S. & Bayliss, O. B. 1970 *Atheroscl.* **11**, 119.

Bell, F. P., Adamson, I. L. & Schwartz, C. J. 1974 *Exp. Mol. Path.* **20**, 57.

Bell, F. P., Gallus, A. S. & Schwartz, C. J. 1974 *Exp. Mol. Path.* **20**, 281.

Bruns, R. R. & Palade, G. E. 1968 *J. Cell Biol.* **37**, 277.

Caro, C. G. 1973 *Atherogenesis: Initiating Factors. Ciba Found. Symp.* no. 12. Assoc. Sci. Publ.

CARO, C. G. 1974 *Cardiovas. Res.* **8**, 194.

CARO, C. G., FITZ-GERALD, J. M. & SCHROTER, R. C. 1971 *Proc. Roy. Soc.* B **177**, 109.

CARO, C. G., LEWIS, C. & WEINBAUM, S. 1974 *Proc. Physiol. Soc.* C **20**, 77.

CARO, C. G. & NEREM, R. M. 1973 *Circul. Res.* **32**, 187.

CARO, C. G., SIFLINGER, A. & PARKER, K. 1975 *Cardiovas. Res.* (in the Press).

CARSLAW, H. S. & JAEGER, J. C. 1959 *Conduction of Heat in Solids*, 2nd edn. Oxford: Clarendon Press.

CASLEY-SMITH, J. R. 1969 *J. Microscopy*, **90**, 15.

CASLEY-SMITH, J. R. & CHIN, J. C. 1971 *J. Microscopy*, **90**, 167.

COX, R. G. & BRENNER, H. 1968 *Chem. Engng Sci.* **22**, 1753.

FRY, D. L. 1968 *Circul. Res.* **22**, 165.

FRY, D. L. 1972 *Circul. Res.* **24**, 93.

FRY, D. L. 1973 *Atherogenesis: Initiating Factors. Ciba Found. Symp.* no. 12. Assoc. Sci. Publ.

GREEN, H. S. & CASLEY-SMITH, J. R. 1972 *J. Theor. Biol.* **35**, 103.

HILLS, B. A. 1968 *Bull. Math. Biophys.* **30**, 47.

HILLS, B. A. 1970 *Bull. Math. Biophys.* **32**, 219.

IRANI, A. R. & ADAMSON, A. W. 1958 *J. Phys. Chem.* **62**, 1517.

ISRAELACHVILI, J. N. & TABOR, D. 1972 *Prog. Surface Membrane Sci.* **7**, 1.

JENNINGS, M. A. & FLOREY, LORD 1967 *Proc. Roy. Soc.* B **167**, 39.

KARNOVSKY, M. J. 1967 *J. Cell Biol.* **37**, 213.

LIFSHITZ, E. M. 1956 *Sov. Phys. Exp. Theor. Phys.* **2**, 73.

PALADE, G. E. 1960 *Anat. Record*, **136**, 254.

SHEA, S. M. & BOSSERT, W. H. 1973 *Microvasc. Res.* **6**, 305.

SHEA, S. M., KARNOVSKY, M. J. & BOSSERT, W. H. 1969 *J. Theor. Biol.* **24**, 30.

SIMIONESCU, N., SIMIONESCU, M. & PALADE, G. E. 1973 *J. Cell Biol.* **57**, 434.

SOMER, J. B. & SCHWARTZ, C. J. 1971 *Atherosclerosis*, **13**, 293.

TAYLOR, E. W. 1965 *Proc. 4th Int. Cong. Rheol.*, part 4. *Symp. Biorheol.* Interscience.

TOMLIN, S. G. 1969 *Biochem. Biophys. Acta*, **183**, 559.

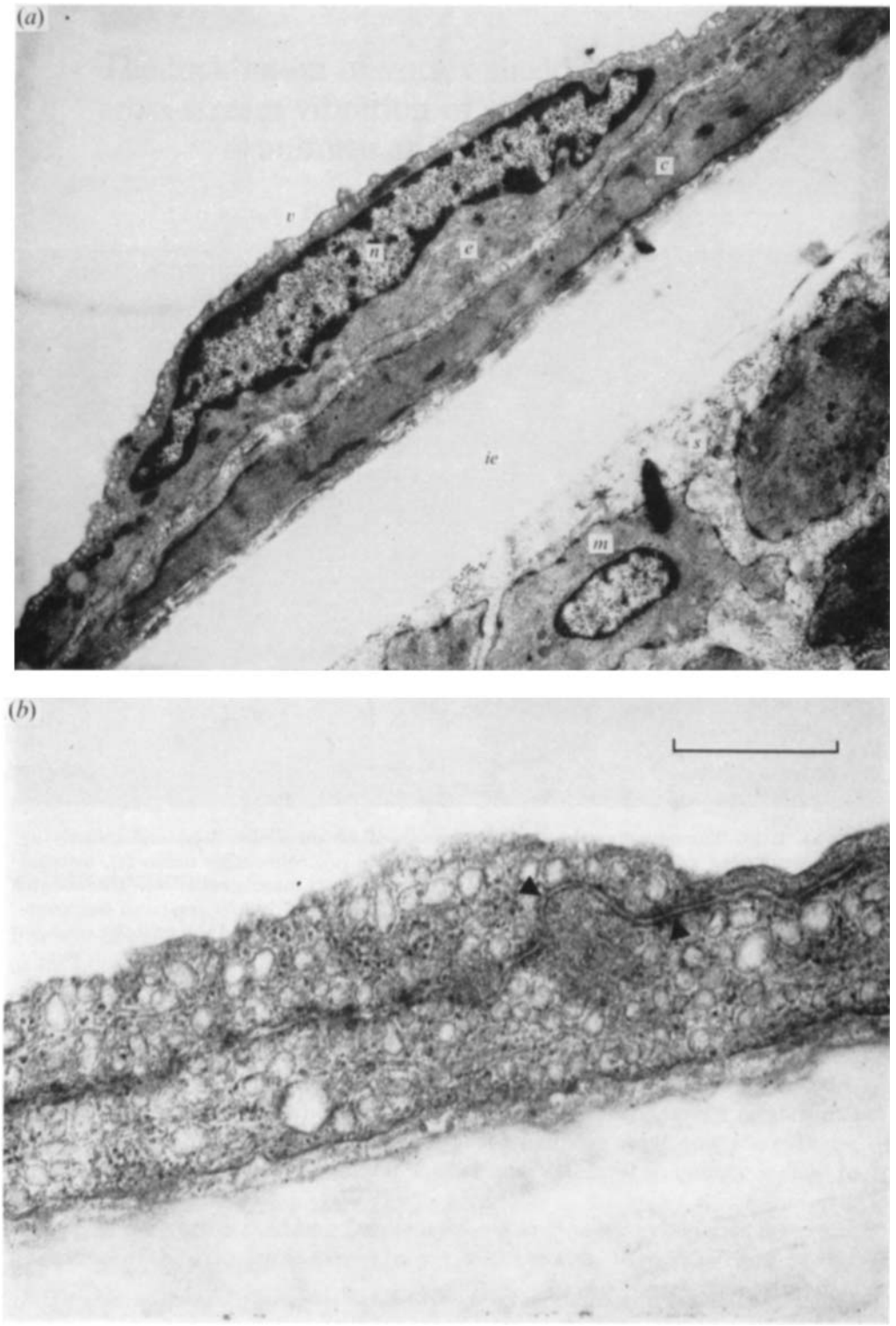

FIGURES 1 (*a*) and (*b*). For (*c*) and legend see over page.

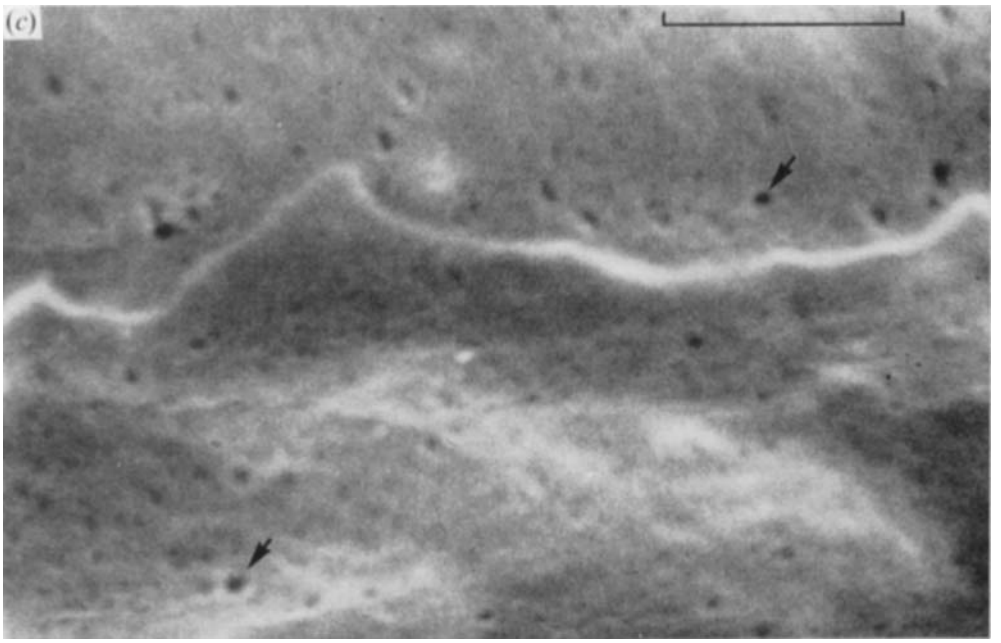

FIGURE 1. (*a*) Transmission electron micrograph of endothelial cell (*e*) and underlying tissue structure, × 17 000: nucleus (*n*), 700 Å vesicle (*v*), connective tissue (*c*), internal elastic lamella (*ie*), interstitial fluid space (*s*) and smooth muscle cells (*m*). Transmural pressure 100 mmHg. (*b*) Transmission electron micrograph of border region of two overlapping endothelial cells showing free migration of 700 Å vesicles and intercellular channel (arrow). Transmural pressure = 300 mmHg. Bar = 0·5 μm. (*c*) Scanning electron micrograph showing border region of two endothelial cells, with openings of attached plasmalemma vesicles (arrows) and depressions indicating attractive London-van der Waals force interaction between vesicles and plasmalemma prior to attachment. Transmural pressure = 100 mmHg. Bar = 0·2 μm.